Stem Cell Reports
Article

ISSCR

OPEN ACCESS

Interleukin-6 Regulates Adult Neural Stem Cell Numbers during Normal and Abnormal Post-natal Development

Mekayla A. Storer,[1] Denis Gallagher,[1,5] Michael P. Fatt,[1,2] Jaclin V. Simonetta,[1,3] David R. Kaplan,[1,2,3,*] and Freda D. Miller[1,2,3,4,*]

[1]Program in Neurosciences and Mental Health, Hospital for Sick Children, Toronto M5G 1L7, Canada
[2]Institute of Medical Science, University of Toronto, Toronto M5G 1A8, Canada
[3]Department of Molecular Genetics, University of Toronto, Toronto M5G 1A8, Canada
[4]Department of Physiology, University of Toronto, Toronto M5G 1A8, Canada
[5]Present address: Create Fertility Clinic, 790 Bay Street, Suite 1100, Toronto M5G 1N8, Canada
*Correspondence: dkaplan@sickkids.ca (D.R.K.), fredam@sickkids.ca (F.D.M.)
https://doi.org/10.1016/j.stemcr.2018.03.008

SUMMARY

Circulating systemic factors can regulate adult neural stem cell (NSC) biology, but the identity of these circulating cues is still being defined. Here, we have focused on the cytokine interleukin-6 (IL-6), since increased circulating levels of IL-6 are associated with neural pathologies such as autism and bipolar disorder. We show that IL-6 promotes proliferation of post-natal murine forebrain NSCs and that, when the IL-6 receptor is inducibly knocked out in post-natal or adult neural precursors, this causes a long-term decrease in forebrain NSCs. Moreover, a transient circulating surge of IL-6 in perinatal or adult mice causes an acute increase in neural precursor proliferation followed by long-term depletion of adult NSC pools. Thus, IL-6 signaling is both necessary and sufficient for adult NSC self-renewal, and acute perturbations in circulating IL-6, as observed in many pathological situations, have long-lasting effects on the size of adult NSC pools.

INTRODUCTION

The ventricular-subventricular zone (V-SVZ) of the lateral ventricles is one of two well-characterized niches for neural stem cells (NSCs) in the post-natal mammalian brain. These V-SVZ NSCs generate neurons, oligodendrocytes, and astrocytes, and this ongoing cell genesis is functionally important (Lim and Alvarez-Buylla, 2016). Since the number of NSCs is a key determinant of the level of cell genesis, it is important to understand the mechanisms that determine adult NSC pool size. In this regard, while post-natal NSC numbers are initially determined developmentally, NSC maintenance is regulated by environmental cues that they are exposed to throughout life.

What then are the environmental cues that regulate adult NSC numbers? Many of the relevant factors derive directly from the local stem cell niche (Miller and Gauthier-Fisher, 2009). For example, V-SVZ NSCs are exposed to the cerebrospinal fluid and to afferent serotonergic axons, both of which are thought to regulate their biology (Silva-Vargas et al., 2016; Tong et al., 2014). These niche effects are likely mediated by neurotransmitters such as serotonin and diffusible growth factors including the glycoprotein 130 (gp130) family of cytokines (Shimazaki et al., 2001; Bauer and Patterson, 2006). In addition, systemic, circulating factors regulate adult NSCs, as shown in parabiosis experiments where the blood of young mice rejuvenated the aged V-SVZ NSC niche, and, conversely, the circulation of an aged mouse reduced neurogenesis in younger mice (Villeda et al., 2011; Katsimpardi et al., 2014). Although circulating GDF11 and CCL11 were identified as mediating the observed effects in part, these studies raise the intriguing possibility that other circulating factors might regulate NSC biology.

One source of potential circulating factors is the immune system, which, when activated, is thought to contribute to neural pathology and degeneration throughout life (Patterson, 2009; Labzin et al., 2017). For example, maternal immune activation due to viral infection causes aberrant behavioral outcomes in offspring, and this is thought to be due to increased circulating interleukin-6 (IL-6) (Patterson, 2009; Smith et al., 2007; Hsiao et al., 2012). In this regard, we previously showed that a transient surge of circulating maternal IL-6 caused long-lasting changes in adult NSCs, in part due to hyper-activation of an endogenous IL-6-dependent self-renewal pathway in embryonic forebrain precursors (Gallagher et al., 2013). Since alterations in circulating IL-6 in humans occur during stress, neurodegeneration, and neuropsychiatric disorders (Mogi et al., 1994; Rohleder et al., 2012; Munkholm et al., 2015; Ashwood et al., 2011), then this raises the possibility that IL-6 might provide one way whereby these pathological conditions could directly affect post-natal NSCs. Here we have addressed this possibility and show that an IL-6/IL-6 receptor pathway is essential for post-natal V-SVZ NSC numbers and that a transient surge of circulating IL-6 acutely activates NSCs in the short term, but ultimately causes NSC depletion in the long term. Thus, perturbations in circulating IL-6, as observed in human pathological conditions, might have long-lasting

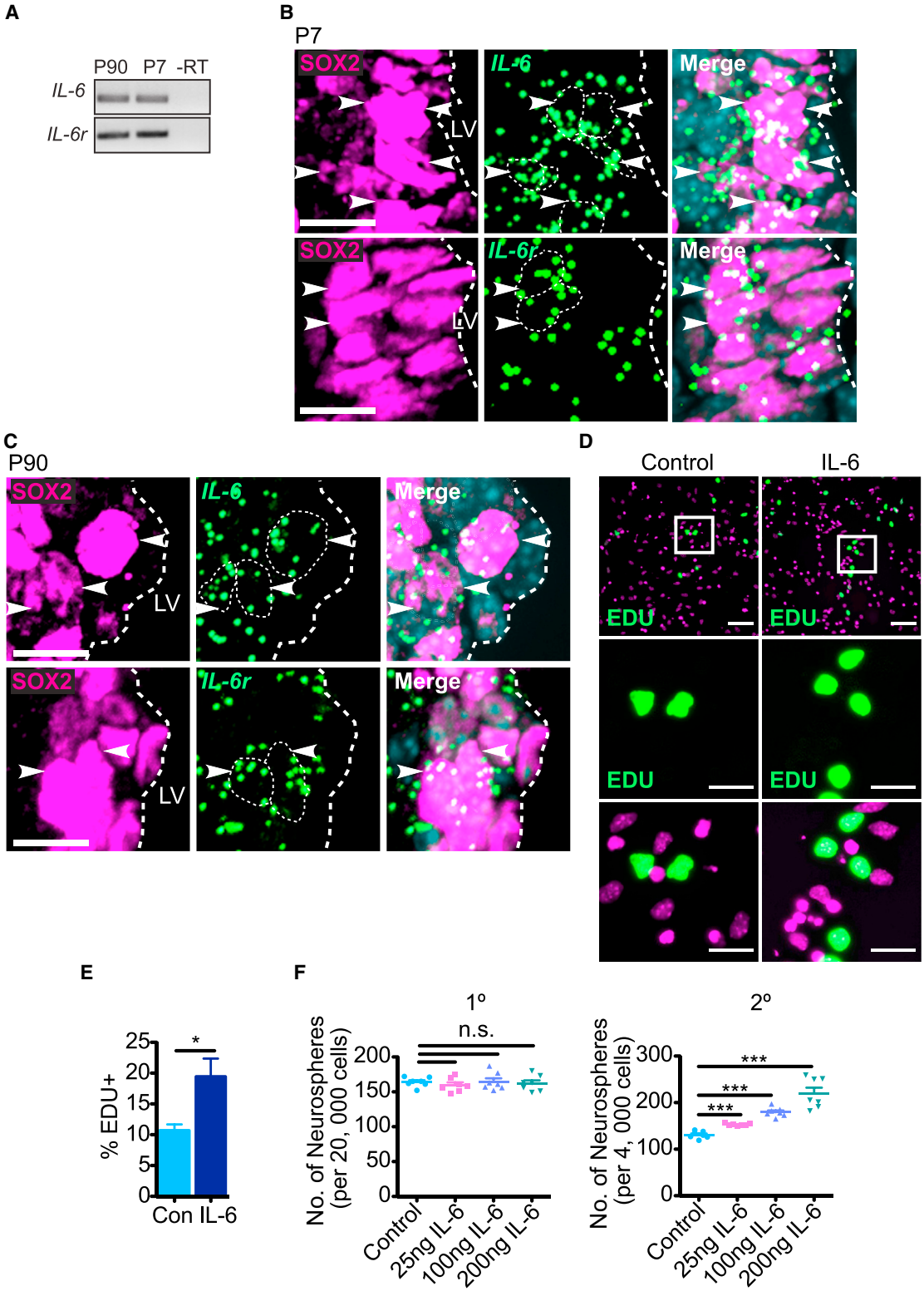

Figure 1. Post-natal V-SVZ Neural Precursor Cells Express IL-6 and IL-6r mRNAs and Respond to IL-6

(A) RT-PCR for *IL-6* (top) and *IL-6r* (bottom) mRNAs in equal amounts of RNA from primary P7 and P90 V-SVZ neurospheres. –RT denotes no reverse transcriptase.

(legend continued on next page)

effects on NSC pools, adult neural cell genesis, and potentially even cognitive outcomes.

RESULTS

Post-natal V-SVZ Neural Precursors Express IL-6 and IL-6R and Respond to Exogenous IL-6

We first asked whether IL-6 or IL-6 receptor α (IL-6R), the IL-6-specific component of the IL-6R/gp130 receptor complex, were expressed in neural precursor cells in the V-SVZ of the lateral ventricles of post-natal day 7 (P7) or adult mice using two approaches. First, we cultured V-SVZ neural precursor cells as primary neurospheres for 1 week and performed RT-PCRs. *IL-6* and *IL-6r* mRNAs were detectably expressed in neurospheres at both ages (Figure 1A). Second, we performed single-molecule fluorescent *in situ* hybridization (FISH), combining it with immunostaining for the pan-neural precursor marker SOX2. *IL-6* and *IL-6r* mRNA were expressed in many SOX2-positive cells in the P7 and adult V-SVZ (Figures 1B and 1C). We demonstrated the specificity of the FISH by performing positive and negative controls (Figure S1).

We next asked if post-natal V-SVZ neural precursor cells responded to exogenous IL-6 in culture. To do so, we generated primary P7 V-SVZ neurospheres, plated these cells adherently in fibroblast growth factor 2 (FGF2) with or without 100 ng/mL IL-6, and 1 day later added 5-ethynyl-2′-deoxyuridine (EdU) and immunostained these cultures 24 hr later. IL-6 increased the proportion of EdU-positive cells from 10% to 20% (Figures 1D and 1E). As a second approach, we cultured adult (P90) V-SVZ cells under neurosphere-initiating conditions in FGF2 and epidermal growth factor (EGF), and added various concentrations of IL-6 on day 5. Two days later, we passaged the neurosphere cells at equal cell densities into FGF2 and EGF without IL-6. Quantification showed that IL-6 had no effect on primary neurosphere numbers, but that it increased secondary neurosphere numbers in a concentration-dependent fashion (Figure 1F), a result indicative of increased self-renewal. Thus, some post-natal V-SVZ neurosphere cells, potentially NSCs, respond to exogenous IL-6 with increased proliferation and self-renewal.

IL-6R Regulates the Number of Post-natal V-SVZ Neural Precursor Cells

To ask if IL-6 is also necessary for neural precursor proliferation and/or self-renewal *in vivo*, we examined mice carrying a floxed *IL-6r* gene, since this receptor is necessary for IL-6 signaling, and IL-6 is its only known ligand. We crossed the *IL-6r*$^{fl/fl}$ mice to *Nestin-CreERT2* mice that also carried a *YFP* transgene with an upstream floxed stop codon in the *Rosa26* locus. When these crossed mice are injected with tamoxifen, this causes deletion of *IL-6r* and expression of the *YFP* reporter in Nestin-positive neural precursors. Using these mice, we asked about a potential role for IL-6R perinatally. Newborn mice were exposed to tamoxifen via their mother's milk at P1–3 and the V-SVZ was analyzed at P8 (Figure 2A). As controls, we analyzed littermates that did not carry the *Nestin-CreERT2* transgene. We confirmed that this treatment caused recombination in neural precursor cells by immunostaining for YFP (Figure 2B); approximately 97% of SOX2-positive cells were YFP positive. We then immunostained similar sections for SOX2 and either GFAP to detect NSCs (Figure 2C) or MASH1 to detect transit-amplifying (TA) cells (Figure 2D). Since cytoplasmic YFP is also expressed in neural precursor cells (although it is undetectable without amplification by immunostaining), we immunostained for the nuclear protein SOX2 in the green channel. Quantification demonstrated that total SOX2-positive V-SVZ neural precursors were decreased about 15% by inducible *IL-6r* deletion (Figure 2E). This decrease was reflective of a selective loss of NSCs, since SOX2-positive, GFAP-positive NSCs were significantly reduced (Figure 2F), while SOX2-positive, MASH1-positive TA cells were not significantly changed (Figure 2G).

To ask if the observed decrease in perinatal NSC numbers was coincident with decreased neural precursor cell proliferation, we exposed P1–P3 mice to tamoxifen, injected them

(B and C) Images of coronal P7 (B) or P90 (C) V-SVZ sections analyzed by SOX2 immunostaining (magenta, left) single-molecule FISH for *IL-6* (top) or *IL-6r* (bottom) mRNAs (green dots), and counterstaining with Hoechst 33258 (light blue, merges). The white hatched lines outline the border of the lateral ventricles (LV). Scale bars, 10 μm.

(D) Images of P7 primary neurosphere cells that were plated adherently with (right) or without (left) 100 ng/mL IL-6, exposed to EdU at 24 hr, and 1 day later immunostained for EdU (green) and counterstained with Hoechst 33258 (magenta). White boxes (top) are shown at higher magnification in the middle and bottom panels. Scale bars, 50 μm (top) and 20 μm (middle and bottom).

(E) Quantification of experiments as in (D), showing the percentage of EdU-positive nuclei with IL-6 or without (Con). *$p < 0.05$; n = 8 mice per group, each cultured independently.

(F) P90 V-SVZ cells were cultured under neurosphere-initiating conditions with no IL-6 (Control) or with 25, 100, or 200 ng/mL IL-6 added on day 5. Primary neurospheres were quantified after an additional 2 days (left graph), cells were passaged at equal densities into EGF and FGF2 alone, and secondary neurospheres were quantified 6 days later (right graph). n.s., not significant, ***$p < 0.001$; n = 7 animals/group, cultured individually in three independent experiments. Error bars represent SEM.

See also Figure S1.

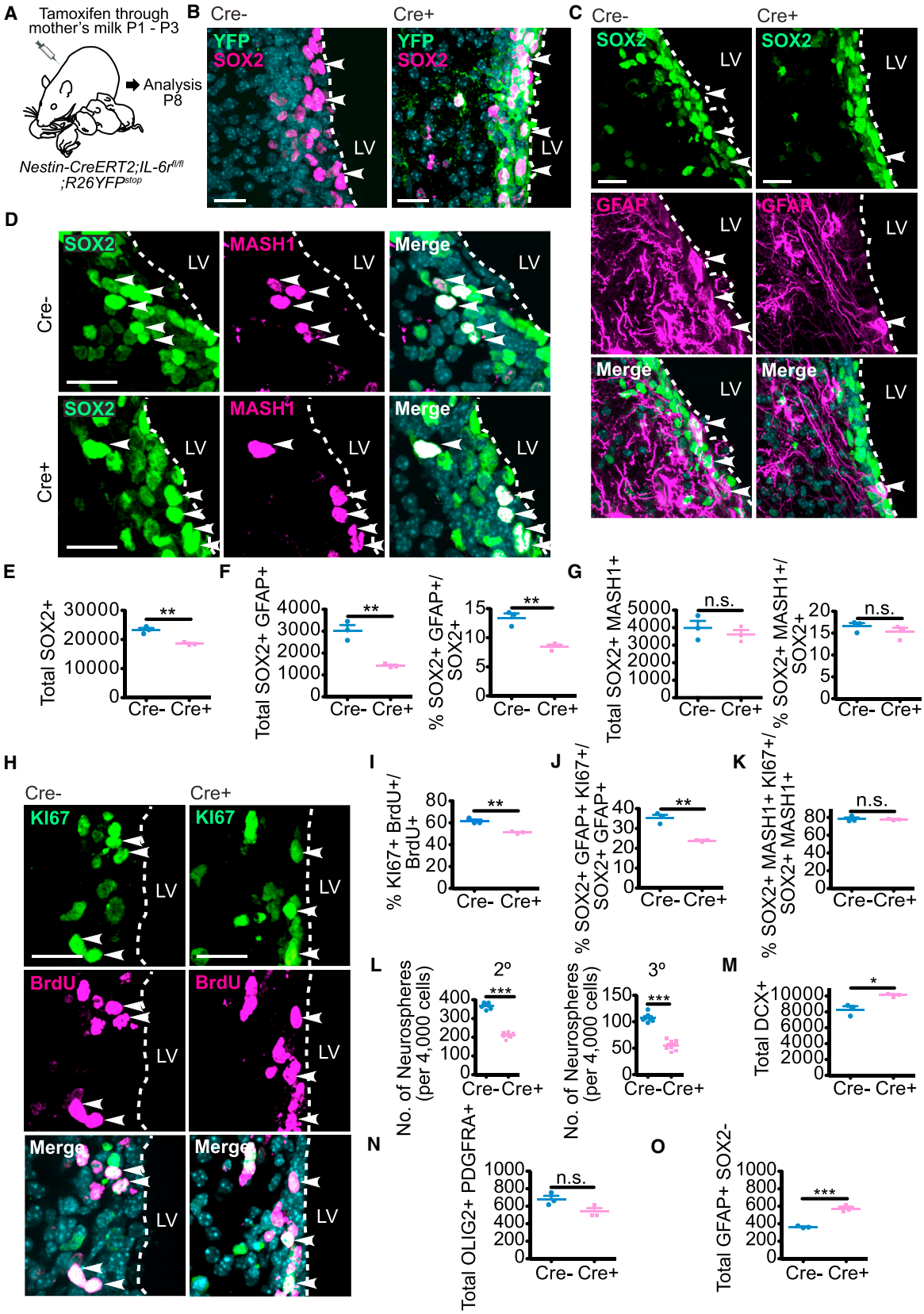

(legend on next page)

with bromodeoxyuridine (BrdU) at P7, and immunostained V-SVZ sections 1 day later for BrdU and the proliferation marker KI67 (Figure 2H). Relative to controls, *IL-6r* deletion significantly decreased the proportion of BrdU-positive V-SVZ cells that were positive for KI67 (Figure 2I). Moreover, triple labeling (Figures S2A and S2B) demonstrated that the proportion of SOX2-positive, GFAP-positive cells that were also KI67-positive was reduced, but that proliferating KI67-positive, SOX2-positive, MASH1-positive TA cells were unaltered (Figures 2J and 2K).

As another measure of neural precursor cell numbers and self-renewal, we cultured primary neurospheres from the P7 V-SVZ of *Nestin-CreERT2;IL-6r*$^{fl/fl}$ mice or their *Nestin-CreERT2; IL-6r*$^{+/+}$ littermates, added tamoxifen from days 5 to 7, and then passaged the cells. There was a significant 57% reduction in secondary neurospheres following inducible *IL-6r* deletion (Figure 2L). Similar results were obtained when these were passaged to generate tertiary neurospheres (Figure 2L). Thus, acute loss of IL-6 signaling in the first post-natal week reduces NSC numbers, likely due in part to reduced self-renewal.

To ask if neural precursor cell differentiation was also altered, we immunostained the P8 V-SVZ of *Nestin-CreERT2;IL-6r*$^{fl/fl}$ mice exposed to tamoxifen from P1 to P3 for DOUBLECORTIN, a marker for newborn neuroblasts/neurons (Figure S2C), or for OLIG2 and PDGFRA to identify newborn oligodendrocyte precursor cells (OPCs) (Figure S2D). This analysis showed that OPCs were not significantly altered (Figure 2N), but that the number of DOUBLECORTIN-positive neuroblasts/neurons was significantly increased by inducible *IL-6r* deletion (Figure 2M). We also analyzed astrocytes, which are positive for GFAP, but negative for SOX2. V-SVZ astrocytes were significantly increased following *IL-6r* deletion (Figure 2O). Thus, loss of IL-6R in nestin-positive neural precursors depletes post-natal V-SVZ NSCs coincident with enhanced neurogenesis and astrogenesis.

IL-6R Is Required for the Long-Term Maintenance of Adult V-SVZ NSCs

To ask if IL-6R is important for NSCs throughout life, we injected adult *Nestin-CreERT2;IL-6r*$^{fl/fl}$*;R26YFP*^{stop} mice with tamoxifen from P60 to P64, and analyzed the V-SVZ at P80 (Figure 3A). As controls, we used mice that carried *Nestin-CreERT2* and *R26YFP*^{stop} but were wild-type (WT) for *IL-6r*. Immunostaining demonstrated that, as seen in neonates, inducible *IL-6r* deletion significantly decreased total SOX2-positive neural precursors at P80 (Figures 3B and 3C). Moreover, SOX2-positive, GFAP-positive NSCs were decreased by about half (Figures 3B and 3D), while SOX2-positive, MASH1-positive TA cells were not significantly changed (Figures 3E and 3F).

To ask if this selective loss of adult NSCs was coincident with decreased proliferation, we injected adult mice with tamoxifen from P60 to P64 and with BrdU at P79. Immunostaining 1 day later showed that inducible deletion of *IL-6r* caused an approximately 2-fold decrease in BrdU-positive cells that were also KI67 positive (Figures 3G and 3H).

Figure 2. IL-6R Is Required for Proliferation and Maintenance of Perinatal V-SVZ NSCs

(A) Schematic of experiments in (B)–(K) and (M)–(O). P1–P3 *Nestin-CreERT2;IL-6r*$^{fl/fl}$*;R26YFP*^{stop} mice (Cre+) or their *IL-6r*$^{fl/fl}$*;R26YFP*^{stop} (Cre−) littermates were exposed to tamoxifen via their mother's milk, injected with BrdU at P7 and analyzed at P8.

(B) Images of coronal P8 V-SVZ sections immunostained for YFP (green) and SOX2 (magenta). Arrowheads denote single- (left) or double- (right) positive cells.

(C and D) Images of coronal P8 V-SVZ sections immunostained for SOX2 (green) and GFAP (C) (magenta), or MASH1 (D) (magenta). Arrowheads denote double-labeled cells.

(E and F) Quantification of sections as in (C) for total SOX2-positive cells (E), total SOX2-positive, GFAP-positive cells (F) (left), or the percentage of SOX2-positive cells expressing GFAP (F) (right). **p < 0.01; n = 3 mice each.

(G) Quantification of sections as in (D) for total SOX2-positive, MASH1-positive cells (left) or the percentage of SOX2-positive cells expressing MASH1 (right). n.s., not significant; n = 3 mice each.

(H) Images of V-SVZ sections immunostained for KI67 (green) and BrdU (magenta). Arrowheads denote double-labeled cells.

(I) Quantification of sections as in (H) for the percentage of BrdU-positive cells expressing KI67. **p < 0.01; n = 3 mice each.

(J and K) Quantification of immunostained P8 V-SVZ sections for the percentage of SOX2-positive, GFAP-positive NSCs (J) or SOX2-positive, MASH1-positive transit-amplifying (TA) cells (K) expressing KI67. n.s., not significant, **p < 0.01; n = 3 mice each.

(L) Quantification of secondary (2°) or tertiary (3°) neurospheres generated from P8 V-SVZ primary neurospheres that were exposed to tamoxifen on day 5 of culturing. Secondary and tertiary neurospheres were counted on 6 and 5 days post-passaging, respectively. ***p < 0.001; n = 7 Cre− and 9 Cre+ mice, cultured individually in three independent experiments.

(M–O) Quantification of immunostained P8 V-SVZ sections for total DOUBLECORTIN (DCX)-positive neuroblasts/neurons (M), for OLIG2-positive, PDGFRA-positive OPCs (N), or for GFAP-positive, SOX2-negative astrocytes (O). n.s., not significant, *p < 0.05, ***p < 0.001; n = 3 mice each. In scatterplots, individual values are shown as points, with the mean and SEM indicated. Merged images show Hoechst 33258 counterstaining (light blue).

Scale bars, 20 μm.

See also Figure S2.

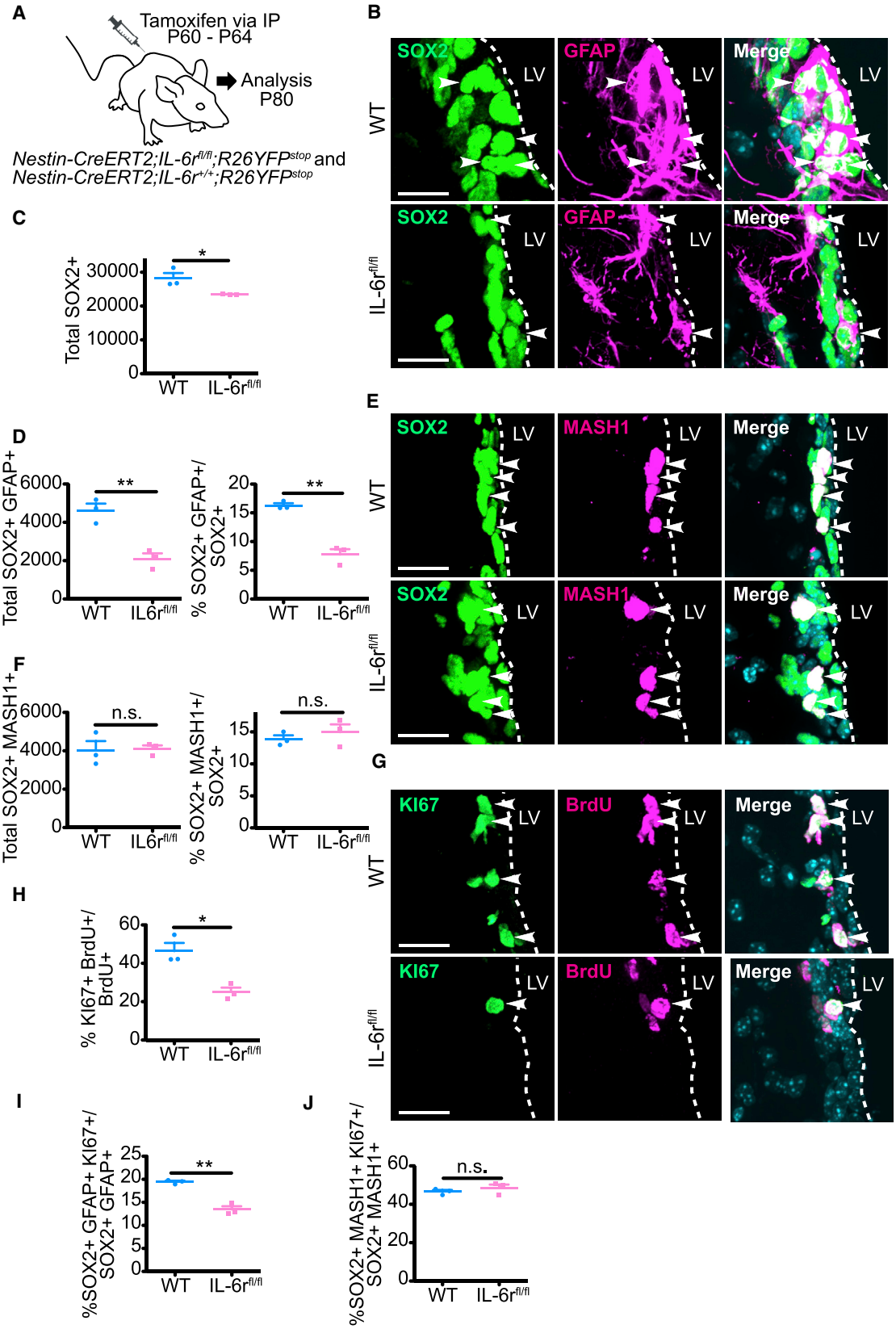

(legend on next page)

Moreover, triple labeling (Figures S3A and S3B) showed that SOX2-positive, GFAP-positive, KI67-positive NSCs were also significantly reduced (Figure 3I), but that proliferating TA cells were unaltered (Figure 3J). Thus, there is an acute, life-long requirement for IL-6R in V-SVZ NSCs for maintenance and proliferation.

IL-6 Is Important for Maintenance of Post-natal V-SVZ NSCs

Since IL-6 is the only known ligand for IL-6R, we asked if it was also necessary for post-natal NSCs by analyzing constitutive adult *IL-6*$^{-/-}$ mice relative to their WT counterparts. Immunostaining demonstrated significant decreases in total SOX2-positive cells and in SOX2-positive, GFAP-positive NSCs in the *IL-6*$^{-/-}$ V-SVZ (Figures 4A–4C). By contrast, SOX2-positive, MASH1-positive TA cells were similar in both groups (Figures 4D and 4E). Thus, as was seen with inducible *IL-6r* deletion, loss of *IL-6* selectively depleted adult V-SVZ NSCs.

Since IL-6 is expressed by SOX2-positive V-SVZ cells (Figures 1B and 1C), we next asked whether some of the IL-6, important for activation of IL-6R on forebrain NSCs, originates within the V-SVZ itself. To do this, we cultured neurospheres from the P7 V-SVZ, and passaged them into FGF2 and EGF with either a previously characterized function-blocking IL-6 antibody (Gallagher et al., 2013) or a control immunoglobulin G (IgG) (Figure 4F). Analysis 6 days later demonstrated a significant 27% decrease in neurospheres with anti-IL-6 (Figure 4G), suggesting that neural precursors themselves are a biologically relevant source of IL-6 in the V-SVZ.

Increased Circulating IL-6 Causes Proliferation of Post-natal V-SVZ NSCs and Expansion of Their TA Cell Progeny in the Short Term

IL-6 crosses the blood-brain barrier (Banks et al., 1994), and circulating levels of IL-6 are known to increase following various systemic challenges. We therefore asked if circulating IL-6 might influence post-natal NSCs by injecting P7 mice intraperitoneally (i.p.) with either IL-6 or PBS vehicle (Figure 5A). Western blot analysis 24 hr later demonstrated that V-SVZ levels of the activated, phosphorylated downstream IL-6R target STAT3 were increased (Figure 5B), supporting the idea that circulating IL-6 can directly access the V-SVZ. We then asked if this IL-6R activation had any biological effects on the V-SVZ 2 days post-injection. Immunostaining showed that the surge of circulating IL-6 increased total SOX2-positive V-SVZ cells (Figures 5C and 5D), and that this was due to increases in both SOX2-positive, GFAP-positive NSCs and SOX2-positive, MASH1-positive TA cells (Figures 5C–5G). We also quantified GFAP-positive, SOX2-negative astrocytes in the V-SVZ, since IL-6 family cytokines are known to increase astrogenesis (Barnabé-Heider et al., 2005). Consistent with this, V-SVZ astrocytes were increased in IL-6-injected mice (Figure 5H).

To ask if the proliferation of neural precursors was also increased, we injected P7 mice with IL-6 and injected them on P8 with BrdU. Immunostaining 1 day later demonstrated that the IL-6 surge increased BrdU-positive, KI67-positive V-SVZ cells from about 30% to almost 50% (Figures 5I and 5J). Moreover, triple labeling showed that proliferating KI67-positive, SOX2-positive, GFAP-positive NSCs were also increased (Figures 5K and 5L). By contrast, the proportion of proliferating SOX2-positive, MASH1-positive TA cells was unaltered by the IL-6 injection (Figures 5M and S4), suggesting that more TA cells were being generated from NSCs, but that their net proliferation rate was unchanged.

As an additional measure of neural precursor cell numbers, we generated primary neurospheres 1 day following IL-6 or PBS injection at P7. This analysis demonstrated a 3- to 4-fold increase in V-SVZ neurosphere-initiating cells following IL-6 injection (Figure 5N). Moreover,

Figure 3. IL-6R Is Required for Maintenance of Adult SVZ Neural Precursor Cell Pools

(A) Schematic of experiments. Adult *Nestin-CreERT2;IL-6r*$^{fl/fl}$*;R26YFP*^{stop} (IL-6r$^{fl/fl}$) or *Nestin-CreERT2;IL-6r*$^{+/+}$*;R26YFP*^{stop} (WT) mice were injected daily from P60 to P64 with tamoxifen, with BrdU on P79, and coronal V-SVZ sections were immunostained at P80.

(B) Images of V-SVZ sections immunostained for SOX2 (green) and GFAP (magenta). Arrowheads denote double-labeled cells.

(C and D) Quantification of sections as in (B) for total SOX2-positive cells (C), SOX2-positive, GFAP-positive cells (D, left), or the percentage of SOX2-positive cells expressing GFAP (D, right). *$p < 0.05$, **$p < 0.01$; n = 3 mice each.

(E) Images of V-SVZ sections immunostained for SOX2 (green) and MASH1 (magenta). Arrowheads denote double-labeled cells.

(F) Quantification of sections as in (E) for total SOX2-positive, MASH1-positive cells (left) and the percentage of SOX2-positive cells expressing MASH1 (right). n.s., not significant; n = 3 mice each.

(G) Images of V-SVZ sections immunostained for KI67 (green) and BrdU (magenta). Arrowheads denote double-labeled cells.

(H) Quantification of sections as in (G) for the percentage of BrdU-positive cells expressing KI67. *$p < 0.05$; n = 3 mice each.

(I and J) Quantification of immunostained V-SVZ sections for the percentage of SOX2-positive, GFAP-positive NSCs (I) or SOX2-positive, MASH1-positive TA cells (J) expressing KI67. n.s., not significant, **$p < 0.01$; n = 3 mice each. In scatterplots, individual values are shown as points, with the mean and SEM indicated. Merged images show Hoechst 33258 counterstaining (light blue).

Scale bars, 20 μm.

See also Figure S3.

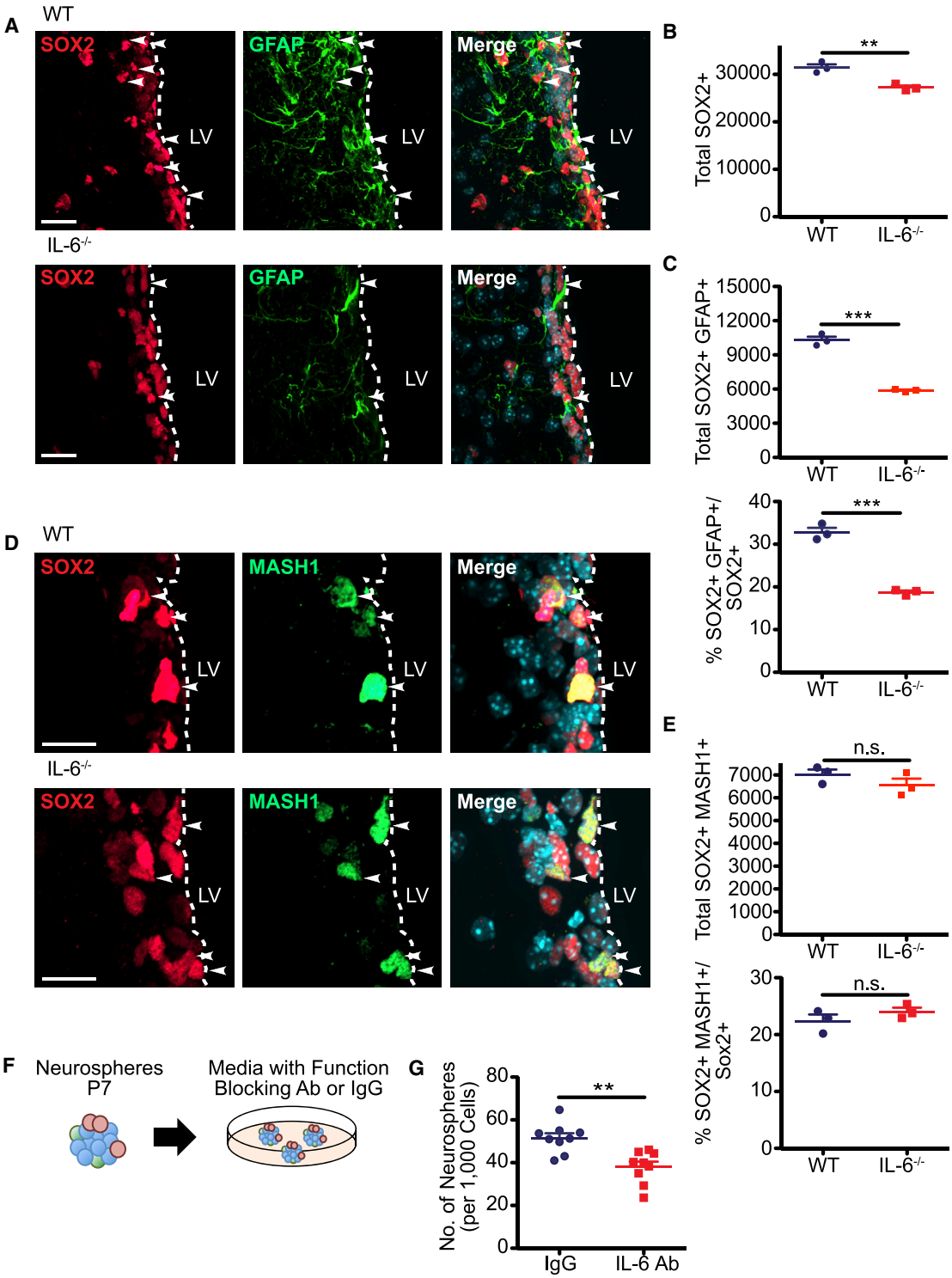

Figure 4. IL-6 Regulates the Size of Post-natal V-SVZ NSC Pools

Coronal sections through the V-SVZ of adult *IL-6*$^{-/-}$ (IL-6$^{-/-}$) or WT control mice were analyzed by immunostaining.

(A) Images of V-SVZ sections immunostained for SOX2 (red) and GFAP (green). Arrowheads denote double-labeled cells.

(B and C) Quantification of sections as in (A) for total SOX2-positive cells (B), total SOX2-positive, GFAP-positive cells (C) (top), and the percentage of SOX2-positive cells expressing GFAP (C) (bottom). **p < 0.01, ***p < 0.001; n = 3 mice each.

(D) Images of V-SVZ sections immunostained for SOX2 (red) and MASH1 (green). Arrowheads denote double-labeled cells.

(legend continued on next page)

almost 2-fold more secondary spheres were generated from the primary neurospheres of IL-6-treated mice (Figure 5O).

Increased Circulating IL-6 Enhances Neurogenesis and Ultimately Causes Depletion of Post-natal V-SVZ NSCs

Subsequently, we asked if the transient increase in circulating IL-6 had longer-term consequences. Initially we asked about olfactory bulb neurogenesis, based upon the rapid IL-6-induced increase in SOX2-positive, MASH1-positive TA cells (Figure 5G). Specifically, we injected P7 mice with IL-6 or PBS, injected them twice with BrdU 1 day later, and analyzed their olfactory bulbs at P21 (Figure 6A). Immunostaining for BrdU and the neuron-specific protein NEUN (Figure 6B) demonstrated that the IL-6 injection caused a significant increase in BrdU-labeled olfactory bulb neurons (Figure 6C).

We then asked whether this acute IL-6-induced burst of NSC proliferation and neurogenesis had any longer-term effect on NSC pools. We injected mice at P7 with IL-6 or PBS and at P21 with BrdU, and then analyzed them 1 day later (Figure 6D). Immunostaining of V-SVZ sections showed that the proportion of BrdU-positive cells that were also KI67 positive was decreased from 34% to 24% in mice injected with IL-6 (Figures 6E and 6F). Consistent with this, total SOX2-positive, GFAP-positive NSCs, and the percentage of these that were KI67 positive, were both significantly reduced (Figures 6H and 6I). By contrast, total and proliferating SOX2-positive, MASH1-positive TA cells were unaffected (Figures 6J–6L) by the earlier surge of circulating IL-6.

To confirm this decrease in neural precursors, we cultured neurospheres from the P21 V-SVZ of mice injected with IL-6 or PBS at P7. There were approximately 2-fold fewer neurosphere-initiating cells in mice injected with IL-6 versus PBS (Figure 6M). Similar decreases were observed upon passaging to generate secondary or tertiary neurospheres (Figures 6N and 6O). Thus, perinatal exposure to increased circulating IL-6 caused an acute increase in NSC proliferation and differentiation, and a deficit in NSC numbers 2 weeks later.

A Surge of Circulating IL-6 Causes Proliferation of Adult V-SVZ NSCs in the Short Term and Depletes Their Numbers in the Long Term

To ask if a circulating IL-6 surge had the same effect in adults, we injected P42 mice with IL-6 or PBS, injected BrdU 1 day later, and analyzed the V-SVZ after an additional day (Figure 7A). IL-6 caused a significant increase in both BrdU-positive, KI67-positive V-SVZ cells (Figures 7B and 7C) and in SOX2-positive, GFAP-positive NSCs (Figures 7D and 7E). By contrast, SOX2-positive, MASH1-positive TA cells were not significantly altered (Figures 7F and 7G). We also asked about differentiation. For astrogenesis, we quantified GFAP-positive, SOX2-negative V-SVZ cells. These astrocytes were not significantly altered by IL-6 injection, although there was a trend to an increase (Figure 7H). To ask about neurogenesis, we injected mice with IL-6 on P42, with BrdU five times on P57, and then analyzed the olfactory bulb at P87. The IL-6 injection caused a small but significant increase in BrdU-positive, NEUN-positive olfactory bulb neurons (Figures 7I and 7J).

Finally, we asked whether the IL-6 surge had longer-term consequences for NSCs by injecting mice with IL-6 or PBS at P42, and analyzing the V-SVZ at P57 (Figure 7K). In IL-6-injected mice, SOX2-positive, GFAP-positive NSCs were significantly decreased (Figures 7L and S5A), as were proliferating KI67-positive, SOX2-positive, GFAP-positive NSCs (Figure 7M). In addition, SOX2-positive, MASH1-positive TA cells were significantly reduced (Figures 7N and S5B), potentially indicating a more direct relationship between NSC numbers and TA cell numbers in the adult versus perinatal V-SVZ. Thus, as was seen in early post-natal mice, a circulating surge of IL-6 in adults transiently increased NSC proliferation and neurogenesis, and ultimately caused a long-term depletion of NSC pools.

DISCUSSION

In humans, circulating IL-6 levels are increased in neuropathological conditions including stress, autism, and neuropsychiatric disorders (Rohleder et al., 2012; Munkholm et al., 2015; Ashwood et al., 2011). Moreover, in a maternal mouse infection model, increased circulating IL-6 causes, in part, adverse behavioral outcomes in progeny (Smith et al., 2007). Here we provide evidence that increased circulating IL-6 can perturb NSC homeostasis in the perinatal and adult murine forebrain, likely by disrupting IL-6R-dependent NSC maintenance, thereby providing a cellular mechanism that could contribute to IL-6-dependent cognitive alterations.

(E) Quantification of sections as in (D) for total SOX2-positive, MASH1-positive cells (top) and the percentage of SOX2-positive cells expressing MASH1 (bottom). n.s., not significant; n = 3 mice each.

(F and G) P7 V-SVZ cells were cultured as neurospheres and, on day 7, cells were passaged into neurosphere medium with either function-blocking IL-6 antibody (IL-6 Ab) or control IgG (F). The number of secondary neurospheres generated from 1,000 cells were counted 6 days later (G).

**$p < 0.01$; n = 9 mice per group, each cultured independently. In scatterplots, individual values are shown as points, with the mean and SEM indicated. Merged images show Hoechst 33258 counterstaining (light blue). Scale bars, 20 μm.

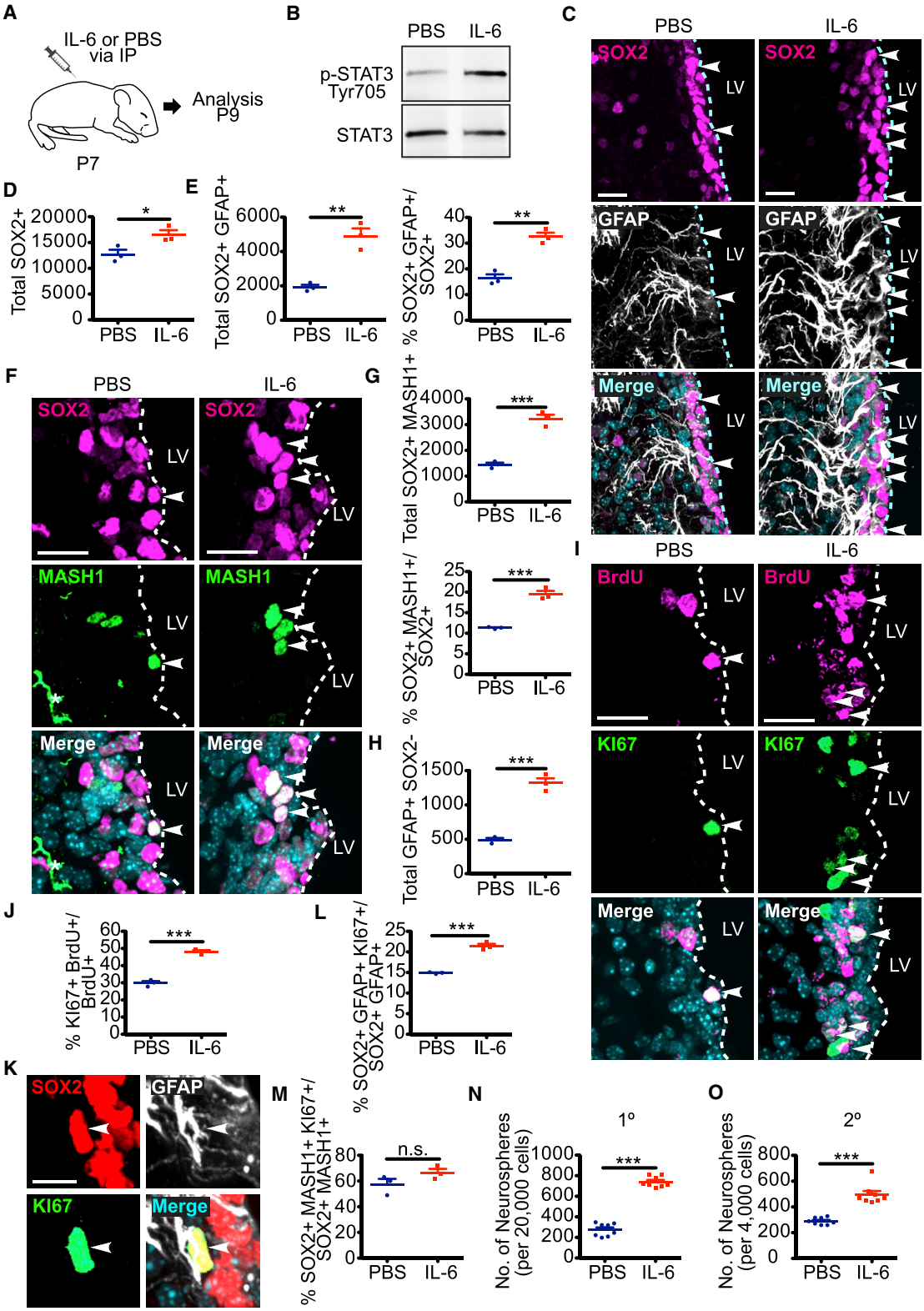

(legend on next page)

Our data show that inducible *IL-6r* deletion in either perinatal or adult nestin-positive neural precursors caused an almost 50% decrease in the numbers and proliferation of V-SVZ NSCs, demonstrating a life-long cell-autonomous requirement for IL-6R in post-natal NSCs. We also demonstrate the converse, that a circulating surge of exogenous IL-6 caused a rapid increase in numbers and proliferation of V-SVZ NSCs. Thus, IL-6R signaling is both necessary and sufficient for self-renewal and maintenance of post-natal V-SVZ NSCs.

The only known ligand for IL-6R is IL-6, and our data show that V-SVZ NSCs are reduced in mice constitutively lacking IL-6. What then is the endogenous source of IL-6? We propose that V-SVZ neural precursors cells themselves are one likely IL-6 source, based upon the function-blocking antibody studies we present here. We also propose that circulating IL-6 is a second important source since (1) we show that peripheral IL-6 injections caused a rapid increase in V-SVZ IL-6R signaling and NSC proliferation, (2) IL-6 crosses the blood-brain barrier (Banks et al., 1994), and (3) there is a close association between forebrain NSCs and blood vessels (Miller and Gauthier-Fisher, 2009). Thus, even under baseline physiological conditions circulating IL-6 might be an important NSC ligand. Moreover, our data clearly demonstrate that when circulating IL-6 is increased as it is in pathological conditions, this deregulates post-natal forebrain NSCs, and, in so doing, potentially disrupts post-natal forebrain development and/or perhaps even contributes to disorders such as schizophrenia (Patterson, 2009).

Although IL-6 is the only IL-6R ligand, this cytokine is a member of a growth factor family that signals through a receptor complex involving gp130 and various ligand-specific receptor components (Heinrich et al., 2003). Intriguingly, two other family members, LIF and CNTF, have also been implicated in self-renewal of adult forebrain NSCs. In particular, overexpression of LIF or infusion of CNTF into the lateral ventricles of mice caused expansion of adult V-SVZ NSCs, while in mice heterozygous for LIF receptor β, a component of the LIF and CNTF receptor complexes, forebrain neural precursor cell proliferation was reduced (Bauer and Patterson, 2006; Shimazaki et al., 2001). These previous studies, together with work reported here, suggest that the maintenance of post-natal V-SVZ NSCs is in part determined by convergent gp130 signaling as initiated by multiple ligands in this family, including IL-6.

Our previous work on IL-6 during forebrain embryogenesis (Gallagher et al., 2013) showed that increased circulating maternal IL-6 during mid-neurogenesis caused rapid proliferation of embryonic forebrain neural precursors and a long-term increase in adult NSC numbers. By contrast, here we demonstrate that a post-natal increase in circulating IL-6 caused an acute increase in proliferation but

Figure 5. Exposure to Increased Circulating IL-6 Acutely Activates Proliferation of Post-natal V-SVZ NSCs and Expands TA Cell Numbers

(A) Schematic of the experimental design. P7 mice were injected with either IL-6 or PBS intraperitoneally and analyzed 1 (B, N, and O) or 2 (C–M) days later. Some mice also received a BrdU injection on P8.

(B) Western blot analysis of equal V-SVZ protein from mice injected with IL-6 or PBS 24 hr earlier, probed with an antibody for phosphorylated, activated STAT3 (Tyr705) (top). The blot was reprobed for total STAT3 (bottom).

(C) Images of V-SVZ sections 2 days post-injection were immunostained for SOX2 (magenta) and GFAP (white). Arrowheads denote double-labeled cells.

(D and E) Quantification of sections as in (C) for total SOX2-positive cells (D), total SOX2-positive, GFAP-positive NSCs (E) (left) and the percentage of SOX2-positive cells expressing GFAP (E) (right). *$p < 0.05$, **$p < 0.01$; n = 3 mice each.

(F) Images of V-SVZ sections immunostained for SOX2 (magenta) and MASH1 (green). Arrowheads denote double-labeled cells and the asterisk indicates an autofluorescent blood vessel.

(G) Quantification of sections as in (F) for total SOX2-positive, MASH1-positive TA cells (top) and the percentage of SOX2-positive cells expressing MASH1 (bottom). ***$p < 0.001$; n = 3 mice each.

(H) Quantification of sections as in (C) for total GFAP-positive V-SVZ astrocytes that were negative for SOX2. ***$p < 0.001$; n = 3 mice each.

(I) Images of V-SVZ sections immunostained for KI67 (green) and BrdU (magenta). Arrowheads denote double-labeled cells.

(J) Quantification of sections as in (I) for the percentage of BrdU-positive cells expressing KI67. ***$p < 0.001$; n = 3 mice each.

(K) Images of a V-SVZ section immunostained for SOX2 (red), GFAP (white), and KI67 (green). The arrowhead denotes a triple-labeled cell.

(L and M) Quantification of immunostained V-SVZ sections for the percentage of SOX2-positive, GFAP-positive NSCs (L) or SOX2-positive, MASH1-positive TA cells (M) expressing KI67. n.s., not significant, ***$p < 0.001$; n = 3 mice each.

(N and O) Quantification of the number of primary (N) (1°) and secondary (O) (2°) neurospheres generated from the V-SVZ of P8 mice injected 24 hr previously with IL-6 or PBS. Neurospheres were counted after 7 days in culture (N) or 6 days post-passaging (O). ***$p < 0.001$; n = 8 mice each, cultured individually in three independent experiments. In scatterplots, individual values are shown as points, with the mean and SEM indicated. Merged images show Hoechst 33258 counterstaining (light blue).

Scale bars, 20 μm except for (K) where they are 10 μm.

See also Figure S4.

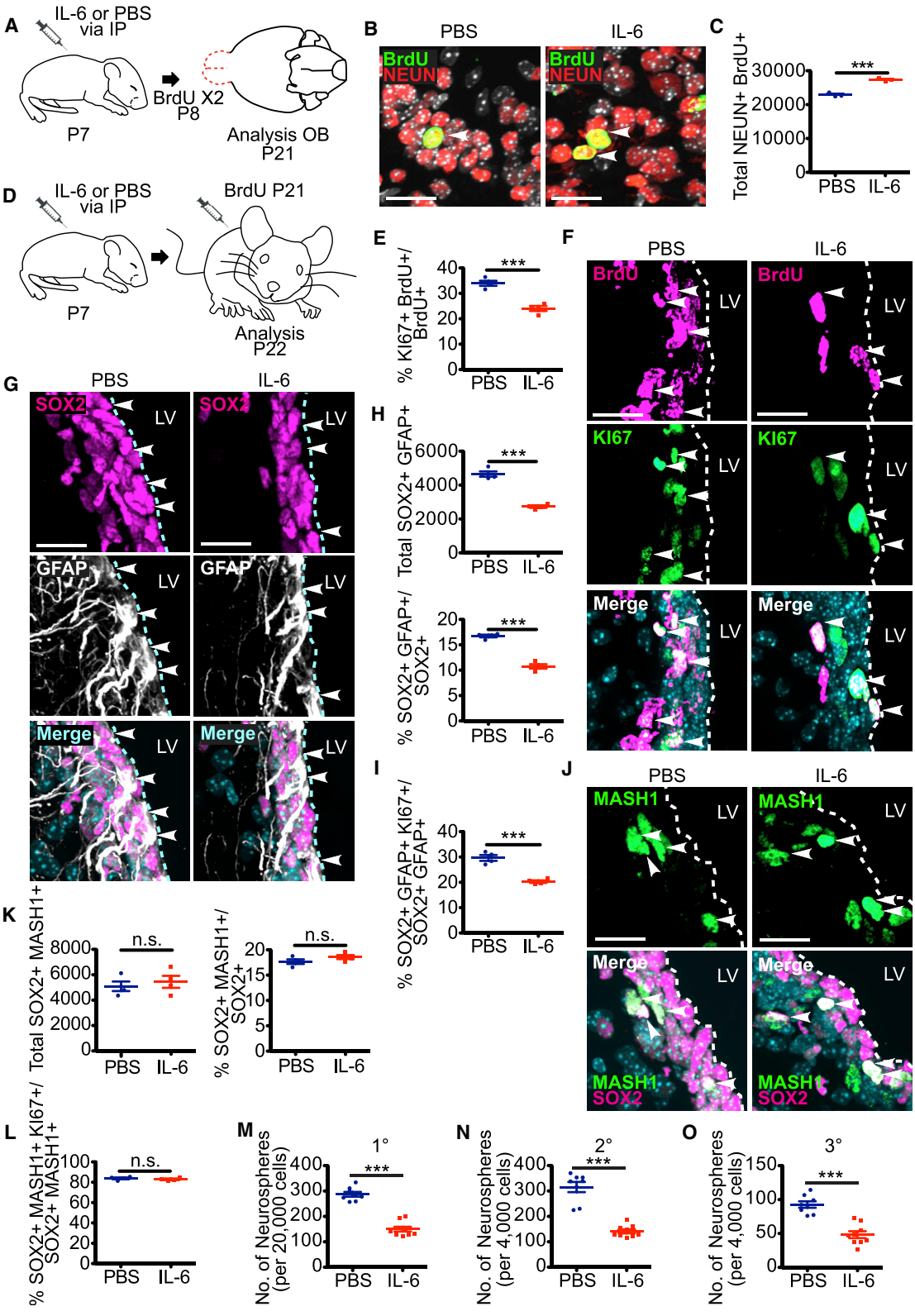

(legend on next page)

ultimately caused long-term depletion of adult NSC pools. We propose that these different long-term outcomes result from differences in neural precursor cell-cycle state since, at the time of the IL-6 surge, embryonic NSCs were actively proliferating while post-natal NSCs were quiescent (Fuentealba et al., 2015; Furutachi et al., 2015; Yuzwa et al., 2017). In particular, we propose that an acute surge of circulating IL-6 prior to quiescence directly translates into more embryonic precursors and ultimately more adult NSCs. By contrast, the same acute surge of circulating IL-6 postnatally likely promotes proliferation of quiescent NSCs, and it might then be difficult and/or impossible for these cells to reacquire a quiescent state. At this later time point, then, the net result would be long-term depletion of quiescent NSCs and perhaps, over time, reductions in the differentiated progeny that are important for maintaining tissue homeostasis. Although this model is speculative, it raises fundamental questions about the nature of the quiescent stem cell state, and has potential repercussions for strategies aimed at mobilizing stem cells for therapeutic purposes.

EXPERIMENTAL PROCEDURES

Animals and Injections

All animal use was approved by The Hospital for Sick Children in accordance with the Canadian Council of Animal Care policies. CD1 mice (Charles River Laboratories) were used unless otherwise indicated. *IL-6r*$^{fl/fl}$ (B6.SJL-IL-6ra$^{tm1.1Drew}$/J, RRID: IMSR_JAX:012944) (McFarland-Mancini et al., 2010), *R26YFP*^{stop} (B6.129X1-Gt(ROSA)26Sor$^{tm1(EYFP)Cos}$/J, RRID: IMSR_JAX:006148) (Srinivas et al., 2001), *Nestin-CreERT2* (C57BL/6-Tg(Nes-cre/ERT2) (Imoyoshi et al., 2006), *IL-6*$^{-/-}$ (B6.129S2- IL-6^{tm1Kopf}/J, RRID: IMSR_JAX:002650) (Kopf et al., 1994), and WT C57BL/6J mice were obtained from The Jackson Laboratory. For perinatal *IL-6r* ablation, 1 day following birth, lactating females were injected i.p. with 1 mg tamoxifen in sunflower oil, twice daily for 3 days. For adult *IL-6r* ablation, mice were injected i.p. daily for 5 days with 100 mg/kg tamoxifen in sunflower oil. For IL-6, adult and perinatal mice were injected i.p. with 5 μg (in 200 μL) and 1 μg (in 50 μL), respectively, of recombinant IL-6 (R&D Systems) dissolved in 0.1% BSA in PBS. Controls were injected with vehicle alone. For acute proliferation experiments, mice were injected once with 100 mg/kg BrdU and analyzed the next day, while for neurogenesis experiments, they were injected with BrdU two (perinatal) or five (adult) times at 2 hr intervals. All mice were bred and genotyped as recommended by The Jackson Laboratory.

Neurosphere Cultures

For neurosphere cultures, the subependyma of the lateral ventricles was dissected and dissociated as described previously (Coles-Takabe et al., 2008) with some modifications described in Supplemental Experimental Procedures. Primary spheres ≥50 μm in diameter were quantified 7 days later. Secondary and tertiary spheres, ≥50 μm in diameter, were quantified 6 and 5 days after passaging, respectively. For genetic ablation experiments, primary neurospheres were generated from *Nestin-CreERT2;IL-6r*$^{fl/fl}$;*R26YFP*^{stop} and *IL-6r*$^{fl/fl}$;*R26YFP*^{stop} P7 littermates and 50 μM tamoxifen, dissolved in DMSO, was added post-plating. For function-blocking antibody experiments, primary neurospheres were cultured for 7 days, passaged, and plated at 2 cells/μL in 24-well

Figure 6. Exposure to Increased Circulating IL-6 Perinatally Enhances Neurogenesis and Ultimately Depletes NSC Pools

(A–C) Mice were injected with IL-6 or PBS on P7, were injected twice with BrdU on P8, and olfactory bulb sections were immunostained on P21 for BrdU (B) (green) and NEUN (B) (red; arrowheads denote double-labeled cells), and double-labeled neurons were quantified (C). ***p < 0.001; n = 3 mice each.

(D) Schematic of the experimental design for (E–L). Mice were injected with either IL-6 or PBS on P7, injected with BrdU on P21 and analyzed on P22.

(E) Quantification of sections as in (F) for the percentage of BrdU-positive cells expressing KI67. ***p < 0.001; n = 4 mice each.

(F and G) Images of V-SVZ sections immunostained for KI67 (F) (green) and BrdU (F) (magenta), or for SOX2 (G) (magenta) and GFAP (G) (white). Arrowheads denote double-labeled cells.

(H) Quantification of sections as in (G) for total SOX2-positive, GFAP-positive cells (top), and for the percentage of SOX2-positive cells expressing GFAP (bottom). ***p < 0.001; n = 4 mice each.

(I) Quantification of immunostained V-SVZ sections for the percentages of SOX2-positive, GFAP-positive NSCs expressing KI67. ***p < 0.001; n = 4 mice each.

(J) Images of V-SVZ sections immunostained for SOX2 (magenta) and MASH1 (green). Arrowheads denote double-labeled cells.

(K) Quantification of sections as in (J) for total SOX2-positive, Mash-positive cells (left) and the percentage of SOX2-positive cells expressing MASH1 (right). n.s., not significant; n = 4 mice each.

(L) Quantification of immunostained V-SVZ sections for the percentage of SOX2-positive, MASH1-positive TA cells expressing KI67. n.s., not significant; n = 4 mice each.

(M–O) Quantification of the number of primary (M) (1°), secondary (N) (2°), and tertiary (O) (3°) neurospheres generated from the V-SVZ of P21 mice injected intraperitoneally 14 days previously with IL-6 or PBS. Neurospheres were counted after 7 days in culture (M) or 6 (N) or 5 (O) days after passaging. ***p < 0.001; n = 8 and 9 PBS and IL-6-injected mice, respectively, all cultured individually in three independent experiments. In scatterplots, individual values are shown as points, with the mean and SEM indicated. Merged images show Hoechst 33258 counterstaining (light blue).

Scale bars, 20 μm.

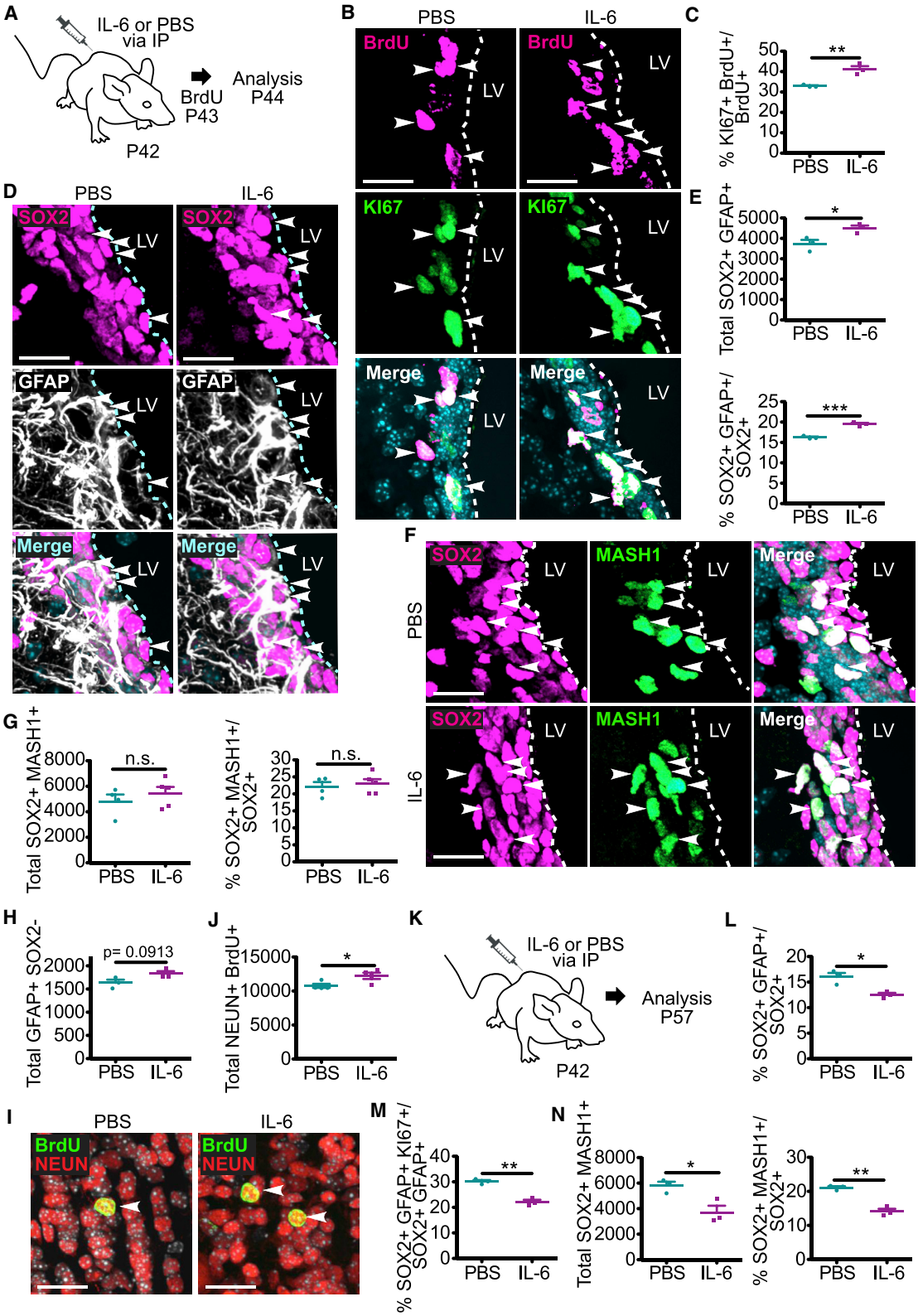

(legend on next page)

plates containing either 10 μg/mL control IgG or IL-6 function-blocking antibody (R&D Systems; Geddes et al., 2011). For proliferation analysis, primary neurospheres were dissociated and plated at a density of 125,000 cells/well in 24-well plates, in triplicate on glass coverslips pre-coated with 2% laminin (BD Biosciences) and 1% poly-D-lysine (Sigma), in serum-free medium containing 2% B27 (Gibco) and 10 ng/mL FGF (Sigma-Aldrich). Twenty-four hours later, 100 ng/mL IL-6 or PBS was added, and 1 day later 10 μM EdU was added. One day later, cultures were fixed with 4% paraformaldehyde and stained for EdU using the Click-iT EdU Alexa Fluor 488 Imaging Kit (Thermo Fisher Scientific) as per manufacturer's instructions.

RT-PCR

Total RNA was isolated from neurospheres after 7 days in culture using the E.Z.N.A. MicroElute Total RNA kits (Omega Bio-tek). Equal amounts of total RNA were reversed-transcribed using the QuantiTect Reverse Transcription Kit (QIAGEN) according to manufacturer's instructions. One-fifth of the RT reaction was used as a template for the RT-PCR amplification using the following gene-specific primers; Murine *GAPDH* forward: GGGTGTGAACCACGA GAAATA, Murine *GADPDH* reverse: CTGTGGTCATGAGCCCTTC, *IL-6* (Bio-Rad, catalog probe: qMmuCID0005613), *IL-6r* (Bio-Rad, catalog probe: qMmuCID0005519). Samples were analyzed in triplicate for at least two separate runs.

FISH

Single-molecule FISH was performed as described (Yuzwa et al., 2016) with probes targeting *IL-6* (GenBank: NM_031168.1), *IL-6r* (GenBank: NM_010559.2), and *Sox2* (GenBank: NM_011443.3) mRNA using the RNAscope kit (Advanced Cell Diagnostics) according to the manufacturer's instructions. The scrambled probe provided with the RNAscope kit was used as a negative control.

Western Blot Analysis

V-SVZ tissue was lysed in radioimmunoprecipitation buffer containing 1× MS-Safe protease and phosphatase inhibitor cocktail (Sigma). Total protein (30 μg) was resolved using 4%–15% gradient Mini-PROTEAN TGX gels (Bio-Rad) according to the manufacturer's protocol, was transferred to nitrocellulose membranes, blocked in 5% BSA (GE Healthcare) and incubated with rabbit anti-p-STAT3 (Tyr705, Cell Signaling Technology, 1:1,000, catalog no. 9145) and mouse anti-STAT3 (Cell Signaling Technology, 1:1,000, catalog no. 9139). Signal was detected using horseradish peroxidase-conjugated secondary antibodies (GE Healthcare), followed by chemiluminescence detection with Amersham ECL substrate (GE Healthcare) and the MicroChemi4.2 system (DNR Bio-Imaging Systems).

Immunocytochemistry, Antibodies, and Microscopy

Immunocytochemistry of frozen tissue sections was performed essentially as described (Voronova et al., 2017) and as detailed in the Supplemental Experimental Procedures. The following primary antibodies were used in this study: goat anti-SOX2 (Santa Cruz, 1:250, catalog no. sc-17320), chicken anti-eGFP (Abcam, 1:1,000, catalog no. ab13970), rat anti-GFAP (Invitrogen, 1:300, catalog no. 130300), mouse anti-MASH1 (BD Pharmingen, 1:1,000, catalog no. 556604), rabbit anti-KI67 (Abcam, 1:250, catalog no. ab15580), rabbit anti-DOUBLECORTIN (Cell Signaling Technology, 1:500, catalog no. 4604), rabbit anti-OLIG2 (Millipore, 1:1,000, catalog no. AB9610), goat anti-PDGFRA (R&D Systems, 1:250, catalog no. AF1062), mouse anti-NEUN (Millipore, 1:500, catalog no. MAB377) and rat anti-BrdU (AbD Serotec, 1:300, catalog no. OBT0030). Fluorescently labeled highly cross-absorbed secondary antibodies were purchased from Jackson ImmunoResearch and used at a dilution of 1:1,000. z-Stacked images were collected using a Quorom Spinning Disk confocal

Figure 7. A Transient Increase in Circulating IL-6 in Adult Mice Increases Proliferating NSCs in the Short Term and Depletes Them in the Long Term

(A) Schematic of the experimental design for (B–H). Mice were injected with IL-6 or PBS on P42, with BrdU 1 day later, and V-SVZ sections were analyzed after an additional day.
(B) Images of V-SVZ sections immunostained for KI67 (green) and BrdU (magenta). Arrowheads denote double-labeled cells.
(C) Quantification of sections as in (B) for the percentage of BrdU-positive cells expressing KI67. **p < 0.01; n = 3 mice each.
(D) Images of V-SVZ sections immunostained for SOX2 (magenta) and GFAP (white). Arrowheads denote double-labeled cells.
(E) Quantification of sections as in (D) for total SOX2-positive, GFAP-positive cells (top) and the percentage of SOX2-positive cells expressing GFAP (bottom). *p < 0.05, ***p < 0.001; n = 3 mice each.
(F) Images of V-SVZ sections immunostained for SOX2 (magenta) and MASH1 (green). Arrowheads denote double-labeled cells.
(G) Quantification of sections as in (F) for total SOX2-positive, MASH1-positive cells (left) and the percentage of SOX2-positive cells expressing MASH1 (right). n.s., not significant; n = 4–5 mice each.
(H) Quantification of sections as in (D) for total GFAP-positive, SOX2-negative astrocytes in the V-SVZ. p = 0.0913; n = 3 mice each.
(I) Images of the olfactory bulbs of P87 mice that were injected with IL-6 or PBS on P42, and then with BrdU five times on P57. Sections were immunostained for BrdU (green) and NEUN (red), and arrowheads denote double-labeled cells.
(J) Quantification of sections as in (I) for total BrdU-positive, NEUN-positive cells per olfactory bulb. *p < 0.05; n = 4 mice each.
(K–N) Adult mice were injected with IL-6 or PBS on P42, V-SVZ sections were immunostained on P57 for SOX2, GFAP, MASH1, and/or KI67 and quantified for the percentage of SOX2-positive cells expressing GFAP (L), the percentage of SOX2-positive, GFAP-positive NSCs expressing KI67 (M), total SOX2-positive, MASH1-positive cells (N) (left), and the percentage of SOX2-positive cells expressing MASH1 (N) (right). *p < 0.05, **p < 0.01; n = 3 mice per group. In scatterplots, individual values are shown as points, with the mean and SEM indicated. Merged images show Hoechst 33258 counterstaining (light blue).
Scale bars, 20 μm. See also Figure S5.

microscope system or a Zeiss Axio Imager M2 system with an X-Cite 120LED light source and a C11440 Hamamatsu camera. Images were taken with an optical slice thickness of 0.3 μm and projected z-stacked images are shown.

Analysis and Statistics

Quantification of immunostained brain and olfactory bulb sections was performed basically as described by Cancino et al. (2013) and explained in more detail in Supplemental Experimental Procedures. For monolayer culture experiments, three to five random fields of view per sample were captured with a 40× objective and quantified, counting at least 200 cells per condition per experiment. All statistical parameters are presented as scatterplots showing means ± SEM. For all datasets, the statistical significance was assessed using a two-tailed unpaired Student's t test where a p value < 0.05 was considered significant. In all cases, Prism (version 5.0a) was used. In figures, asterisks denote statistical significance marked by *$p < 0.05$, **$p < 0.01$, and ***$p < 0.001$. In all figures, all samples or mice were used without exclusion. Sample sizes (n) indicated in the legends of Figures 1D–1F, 2L, 4G, 5N, 5O, and 6M–6O correspond to the number of biological replicates analyzed. Sample sizes (n) indicated in the legends of Figures 2E–2G, 2I–2K, 2M–2O, 3C, 3D, 3F, 3H–3J, 4B–4E, 5D, 5E, 5G, 5H, 5J, 5L, 5M, 6C, 6E, 6H, 6I, 6K, 6L, and 7C, 7E, 7G, 7H, 7J, 7L–7N correspond to the number of brains from at least two litters analyzed.

SUPPLEMENTAL INFORMATION

Supplemental Information includes Supplemental Experimental Procedures and five figures and can be found with this article online at https://doi.org/10.1016/j.stemcr.2018.03.008.

AUTHOR CONTRIBUTIONS

M.A.S. led the project, planned and carried out the experiments, analyzed the data, and co-wrote the paper. D.G. and M.P.F. planned and carried out the experiments and analyzed the data. J.V.S. carried out the experiments. D.R.K. and F.D.M. directed the project, planned the experiments, analyzed the data, and co-wrote the paper.

ACKNOWLEDGMENTS

This work was funded by CIHR grants to F.D.M. and D.R.K. F.D.M. is a Canada Research Chair. M.A.S. is funded by an Ontario Stem Cell Institute fellowship. We thank Sarah Burns and Dennis Aquino for technical assistance and Scott Yuzwa for helpful discussions.

Received: December 7, 2017
Revised: March 8, 2018
Accepted: March 9, 2018
Published: April 5, 2018

REFERENCES

Ashwood, P., Krakowiak, P., Hertz-Picciotto, I., Hansen, R., Pessah, I., and Van de Water, J. (2011). Elevated plasma cytokines in autism spectrum disorders provide evidence of immune dysfunction and are associated with impaired behavioral outcome. Brain Behav. Immun. *25*, 40–45.

Banks, W.A., Kastin, A.J., and Gutierrez, E.G. (1994). Penetration of interleukin-6 across the murine blood-brain barrier. Neurosci. Lett. *179*, 53–56.

Barnabé-Heider, F., Wasylnka, J.A., Fernandes, K.J.L., Porsche, C., Sendtner, M., Kaplan, D.R., and Miller, F.D. (2005). Evidence that embryonic neurons regulate the onset of cortical gliogenesis via cardiotrophin-1. Neuron *48*, 253–265.

Bauer, S., and Patterson, P.H. (2006). Leukemia inhibitory factor promotes neural stem cell self-renewal in the adult brain. J. Neurosci. *26*, 12089–12099.

Cancino, G.I., Yiu, A.P., Fatt, M.P., Dugani, C.B., Flores, E.R., Frankland, P.W., Josselyn, S.A., Miller, F.D., and Kaplan, D.R. (2013). p63 regulates adult neural precursor and newly born neuron survival to control hippocampal-dependent behavior. J. Neurosci. *33*, 12569–12585.

Coles-Takabe, B.L.K., Brain, I., Purpura, K.A., Karpowicz, P., Zandstra, P.W., Morshead, C.M., and van der Kooy, D. (2008). Don't look: growing clonal versus nonclonal neural stem cell colonies. Stem Cells *26*, 2938–2944.

Fuentealba, L.C., Rompani, S.B., Parraguez, J.I., Obernier, K., Romero, R., Cepko, C.L., and Alvarez-Buylla, A. (2015). Embryonic origin of postnatal neural stem cells. Cell *161*, 1644–1655.

Furutachi, S., Miya, H., Watanabe, T., Kawai, H., Yamasaki, N., Harada, Y., Imayoshi, I., Nelson, M., Nakayama, K.I., Hirabayashi, Y., and Gotoh, Y. (2015). Slowly dividing neural progenitors are an embryonic origin of adult neural stem cells. Nat. Neurosci. *18*, 657–665.

Gallagher, D., Norman, A.A., Woodard, C.L., Yang, G., Gauthier-Fisher, A., Fujitani, M., Vessey, J.P., Cancino, G.I., Sachewsky, N., Woltjen, K., et al. (2013). Transient maternal IL-6 mediates long-lasting changes in neural stem cell pools by deregulating an endogenous self-renewal pathway. Cell Stem Cell *13*, 564–576.

Geddes, K., Rubino, S.J., Magalhaes, J.G., Streutker, C., Le Bourhis, L., Cho, J.H., Robertson, S.J., Kim, C.J., Kaul, R., Philpott, D.J., and Girardin, S.E. (2011). Identification of an innate T helper type 17 response to intestinal bacterial pathogens. Nat. Med. *17*, 837–844.

Heinrich, P.C., Behrmann, I., Haan, S., Hermanns, H.M., Muller-Newen, G., and Schaper, F. (2003). Principles of interleukin (IL)-6-type cytokine signaling and its regulation. Biochem. J. *374*, 1–20.

Hsiao, E.Y., McBride, S.W., Chow, J., Mazmanian, S.K., and Patterson, P.H. (2012). Modeling an autism risk factor in mice leads to permanent immune dysregulation. Proc. Natl. Acad. Sci. USA *109*, 12776–12781.

Imoyoshi, I., Ohtsuka, T., Metzger, D., Chambon, P., and Kageyama, R. (2006). Temporal regulation of Cre recombinase activity in neural stem cells. Genesis *44*, 233–238.

Katsimpardi, L., Litterman, N.K., Schein, P.A., Miller, C.M., Loffredo, F.S., Wojtkiewicz, G.R., Chen, J.W., Lee, R.T., Wagers, A.J., and Rubin, L.L. (2014). Vascular and neurogenic rejuvenation of the aging mouse brain by young systemic factors. Science *344*, 630–634.

Kopf, M., Baumann, H., Freer, G., Freudenberg, M., Lamers, M., Kishimoto, T., Zinkernagal, R., Bluethmann, H., and Köhler, G.

(1994). Impaired immune and acute-phase responses in interleukin-6-deficient mice. Nature *368*, 339–342.

Labzin, L.I., Heneka, M.T., and Latz, E. (2017). Innate immunity and neurodegeneration. Annu. Rev. Med. *69*, 437–449.

Lim, D.A., and Alvarez-Buylla, A. (2016). The adult ventricular–subventricular zone (V-SVZ) and olfactory bulb (OB) neurogenesis. Cold Spring Harb. Perspec. Biol. *8*. https://doi.org/10.1101/cshperspect.a018820.

McFarland-Mancini, M.M., Funk, H.M., Paluch, A.M., Zhou, M., Giridhar, P.V., Mercer, C.A., Kozma, S.C., and Drew, A.F. (2010). Differences in wound healing in mice with deficiency of IL-6 versus IL-6 receptor. J. Immunol. *184*, 7219–7228.

Miller, F.D., and Gauthier-Fisher, A. (2009). Home at last: neural stem cell niches defined. Cell Stem Cell *4*, 507–510.

Mogi, M., Harada, M., Kondo, T., Riederer, P., Inagaki, H., Minami, M., and Nagatsu, T. (1994). Interleukin-1 beta, interleukin-6, epidermal growth factor and transforming growth factor-alpha are elevated in the brain from parkinsonian patients. Neurosci. Lett. *180*, 147–150.

Munkholm, K., Weikop, P., Kessing, L.V., and Vinberg, M. (2015). Elevated levels of IL-6 and IL-18 in manic and hypomanic states in rapid cycling bipolar disorder patients. Brain Behav. Immun. *43*, 205–213.

Patterson, P.H. (2009). Immune involvement in schizophrenia and autism: etiology, pathology and animal models. Behav. Brain Res. *204*, 313–321.

Rohleder, N., Aringer, M., and Boentert, M. (2012). Role of interleukin-6 in stress, sleep, and fatigue. Ann. N.Y. Acad. Sci. *1261*, 88–96.

Shimazaki, T., Shingo, T., and Weiss, S. (2001). The ciliary neurotrophic factor/leukemia inhibitory factor/gp130 receptor complex operates in the maintenance of mammalian forebrain neural stem cells. J. Neurosci. *21*, 7642–7653.

Silva-Vargas, V., Maldonado-Soto, A.R., Mizrak, D., Codega, P., and Doetsch, F. (2016). Age-dependent niche signals from the choroid plexus regulate adult neural stem cells. Cell Stem Cell *19*, 643–652.

Smith, S.E.P., Li, J., Garbett, K., Mirnics, K., and Patterson, P.H. (2007). Maternal immune activation alters fetal brain development through interleukin-6. J. Neurosci. *27*, 10695–10702.

Srinivas, S., Watanabe, T., Lin, C.S., William, C.M., Tanabe, Y., Jessell, T.M., and Costantini, F. (2001). Cre reporter strains produced by targeted insertion of EYFP and ECFP into the ROSA26 locus. BMC Dev. Biol. *1*, 4.

Tong, C.K., Chen, J., Cebrián-Silla, A., Mirzadeh, Z., Obernier, K., Guinto, C.D., Tecott, L.H., Garcia-Verdugo, J.M., Kriegstein, A., and Alvarez-Buylla, A. (2014). Axonal control of the adult neural stem cell niche. Cell Stem Cell *14*, 500–511.

Villeda, S.A., Luo, J., Mosher, K.I., Zou, B., Britschgi, M., Bieri, G., Stan, T.M., Fainberg, N., Ding, Z., Eggel, A., et al. (2011). The ageing systemic milieu negatively regulates neurogenesis and cognitive function. Nature *477*, 90–94.

Voronova, A., Yuzwa, S.A., Wang, B.S., Zahr, S., Syal, C., Wang, J., Kaplan, D.R., and Miller, F.D. (2017). Migrating interneurons secrete fractalkine to promote oligodendrocyte formation in the developing mammalian brain. Neuron *94*, 500–516.

Yuzwa, S.A., Yang, G., Borrett, M.J., Clarke, G., Cancino, G.I., Zahr, S.K., Zandstra, P.W., Kaplan, D.R., and Miller, F.D. (2016). Proneurogenic ligands defined by modeling developing cortex growth factor communication networks. Neuron *91*, 988–1004.

Yuzwa, S.A., Borrett, M.J., Innes, B.T., Voronova, A., Ketela, T., Kaplan, D.R., Bader, G.D., and Miller, F.D. (2017). Developmental emergence of adult neural stem cells as revealed by single cell transcriptional profiling. Cell Rep. *21*, 3970–3986.